Rapid screening of engineered microbial therapies in a 3D multicellular model

Tetsuhiro Harimoto[a], Zakary S. Singer[a], Oscar S. Velazquez[a], Joanna Zhang[a], Samuel Castro[a], Taylor E. Hinchliffe[a], William Mather[b], and Tal Danino[a,c,d,1]

[a]Department of Biomedical Engineering, Columbia University, New York, NY 10027; [b]BioCircuits Institute, University of California, San Diego, La Jolla, CA 92093; [c]Data Science Institute, Columbia University, New York, NY 10027; and [d]Herbert Irving Comprehensive Cancer Center, Columbia University, New York, NY 10027

Edited by Charles R. Cantor, Retrotope, Inc., Del Mar, CA, and approved March 18, 2019 (received for review December 20, 2018)

Synthetic biology is transforming therapeutic paradigms by engineering living cells and microbes to intelligently sense and respond to diseases including inflammation, infections, metabolic disorders, and cancer. However, the ability to rapidly engineer new therapies far outpaces the throughput of animal-based testing regimes, creating a major bottleneck for clinical translation. In vitro approaches to address this challenge have been limited in scalability and broad applicability. Here, we present a bacteria-in-spheroid coculture (BSCC) platform that simultaneously tests host species, therapeutic payloads, and synthetic gene circuits of engineered bacteria within multicellular spheroids over a timescale of weeks. Long-term monitoring of bacterial dynamics and disease progression enables quantitative comparison of critical therapeutic parameters such as efficacy and biocontainment. Specifically, we screen *Salmonella typhimurium* strains expressing and delivering a library of antitumor therapeutic molecules via several synthetic gene circuits. We identify candidates exhibiting significant tumor reduction and demonstrate high similarity in their efficacies, using a syngeneic mouse model. Last, we show that our platform can be expanded to dynamically profile diverse microbial species including *Listeria monocytogenes*, *Proteus mirabilis*, and *Escherichia coli* in various host cell types. This high-throughput framework may serve to accelerate synthetic biology for clinical applications and for understanding the host–microbe interactions in disease sites.

synthetic biology | high-throughput screening | bacterial therapy | cancer therapy

The abundance of naturally occurring microbes living in and on the human body present a myriad of opportunities for engineering microbes to act as in situ therapies or diagnostics. As a result, an emerging focus of synthetic biology has been to engineer bacteria to intelligently sense and respond to disease states including inflammation (1, 2), infections (3–5), metabolic disorders (6, 7), and cancer (8). Notably, many bacteria have been found to selectively colonize tumors in vivo, prompting attempts to engineer bacteria as programmable vehicles to deliver anticancer therapeutics (9). Given their natural preference for tumors and capability for genetic engineering of therapeutic payloads and control systems, engineered bacteria present a unique opportunity to develop a targeted and dynamic therapy to improve efficacy and safety profiles compared with conventional systemic chemotherapy. However, a major bottleneck for clinical translation in all these cases has been animal-based testing, which slows iterations of design cycles needed to produce robust microbial systems for in vivo applications. As a consequence, typical development of engineered bacteria occurs in environments far from in vivo conditions, inevitably leading to failure of predicted functions in more stringent native niches (10, 11).

In vitro platforms have been developed to characterize small-molecule drugs and biologics in more physiologically relevant conditions, with examples including organs-on-a-chip, microfabricated cell patterning, and multicellular spheroids and organoids (12–15). These systems allow for growth of cells in three dimensions, which preserves characteristic features of in vivo environments such as gradients in oxygen and metabolites, cell–cell interactions, and intercellular variations compared with 2D monolayer cultures (16). Furthermore, analyses such as drug distribution and spatially heterogeneous responses can be performed that are otherwise unattainable in monolayer systems (17). For bacterial therapies, 3D disease models could provide an ideal testbed for quantitatively monitoring bacterial localization and circuit dynamics that are critical for accurate estimation of safety and efficacy in vivo.

Due to the rapid proliferation rate of bacteria, coculture with mammalian cells has been a challenge, limiting assays to short periods or necessitating the use of heat-killed bacteria (18, 19). Previous attempts to control the imbalance in growth rates have fluidically controlled excess bacteria, directly injected bacteria into multicellular aggregates, or used obligate anaerobes to prevent overgrowth (20–22). As a result, these systems expectedly increase technical complexity and restrict species types, reducing throughput and broad applicability, respectively. Furthermore, long-term analysis of bacteria circuit dynamics has yet to be employed in multicellular cocultures or applied toward therapeutic development (19). To accelerate development for in vivo applications, simple and high-throughput 3D coculture platforms are needed to rapidly identify effective microbial therapy candidates.

Here we present a bacteria-in-spheroid coculture (BSCC) platform to test a large number of engineered microbial therapies

Significance

An emerging area of synthetic biology is the engineering of bacteria to diagnose and treat various diseases in the body. However, the lack of physiologically relevant in vitro testing environments to rapidly screen bacterial therapies limits their development for clinical use. Here, we develop a platform that enables parallel and long-term monitoring of engineered bacteria in multicellular spheroids. Using this system, we rapidly screened tumor-targeting bacteria engineered to deliver a library of anticancer molecules via synthetic gene circuits. We demonstrate high similarity between in vitro and in vivo results and show broad applicability of the system with various bacterial species and cell types. This technology may serve to accelerate future clinical applications for synthetic biology.

Author contributions: T.H., Z.S.S., and T.D. designed research; T.H., Z.S.S., O.S.V., J.Z., S.C., and T.E.H. performed research; W.M. contributed new reagents/analytic tools; T.H., W.M., and T.D. analyzed data; and T.H. and T.D. wrote the paper.

Conflict of interest statement: T.H., Z.S.S., and T.D. have filed a provisional patent application with the US Patent and Trademark Office related to this work.

This article is a PNAS Direct Submission.

Published under the PNAS license.

[1]To whom correspondence should be addressed. Email: td2506@columbia.edu.

This article contains supporting information online at www.pnas.org/lookup/suppl/doi:10.1073/pnas.1820824116/-/DCSupplemental.

Published online April 17, 2019.

www.pnas.org/cgi/doi/10.1073/pnas.1820824116

Downloaded at Palestinian Territory, occupied on December 3, 2021

www.manaraa.com

that can be created from combinations of genetic circuits, therapeutic payloads, and host species in 3D multicellular spheroids (Fig. 1*A*). By selectively confining bacterial growth within spheroids, we enable parallel and stable coculture with diverse bacteria and cell types. Using the BSCC system, we screened clinically relevant *S. typhimurium* delivering a library of anticancer molecules via synthetic gene circuits and identified efficacious therapies for in vivo applications.

Results

Establishing a Stable Bacteria Co-Culture System in Multicellular Spheroids. To rapidly screen microbial therapies, we generated 3D multicellular spheroids in 96-well plates for parallel testing (14) (Movie S1). We first characterized attenuated *S. typhimurium*, a model bacterium well-characterized for its tumor colonization and anticancer applications in vivo (9, 23), and constitutively expressed superfolder GFP (sfGFP) to track its dynamics. To confine bacteria within spheroids without causing cell toxicity, we screened several antimicrobial agents (*SI Appendix*, Table S1) and developed a coculture protocol using gentamicin, a broad-spectrum aminoglycoside with reduced permeability through the eukaryotic membrane (24) (*SI Appendix*, Fig. S1). Here, bacteria infiltrated spheroids and subsequently localized and proliferated specifically in the spheroid (Movie S2). When no gentamicin was used, bacteria grew rapidly in the surrounding culture media (Movie S3). To investigate the spatiotemporal dynamics of bacteria in detail, we used automated image analysis to quantify the distribution of fluorescence intensity within the spheroid over time. Bacteria fluorescence was initially observed to increase near the spheroid boundary (40 h), reach a steady state level of fluorescence (110 h), and eventually grow and expand within the spheroid (140 h; Fig. 1*B* and *C* and *SI Appendix*, Fig. S2). Bacterial proliferation over time was confirmed by plating dissociated spheroids on selective agar (Fig. 1*C*). Bacteria achieved stable colonization for up to 2 wk and localized to the spheroid core, where necrotic and hypoxic regions developed (Fig. 1*D* and *SI Appendix*, Fig. S2), analogous to bacteria colonization conditions in vivo (25). These results suggest our BSCC platform enables long-term, quantitative characterization of bacterial dynamics within physiologically relevant 3D models in a parallel manner.

Quantitatively Monitoring Synthetic Gene Circuit Dynamics in BSCC. We first sought to characterize gene circuit dynamics designed for in vivo therapeutic delivery, using the BSCC platform. We constructed an acyl-homoserine lactone (AHL)-inducible *luxI* promoter (Fig. 2*A*) and characterized circuit dynamics by monitoring downstream production of sfGFP from *S. typhimurium* within the spheroid. We applied 10 nM AHL to spheroids after bacteria localized within the spheroid, and observed induction in sfGFP signal that reached steady-state expression within 10 h (Fig. 2*A*, *SI Appendix*, Fig. S3, and Movie S4), demonstrating the ability to trigger therapeutic production within a tumor environment. To sustain therapeutic production without repeated infusion of chemical inducer, we next sought to engineer positive feedback from *luxI* to build a quorum-sensing (QS) circuit (Fig. 2*B*). This circuit enables self-triggered gene expression when bacteria reach

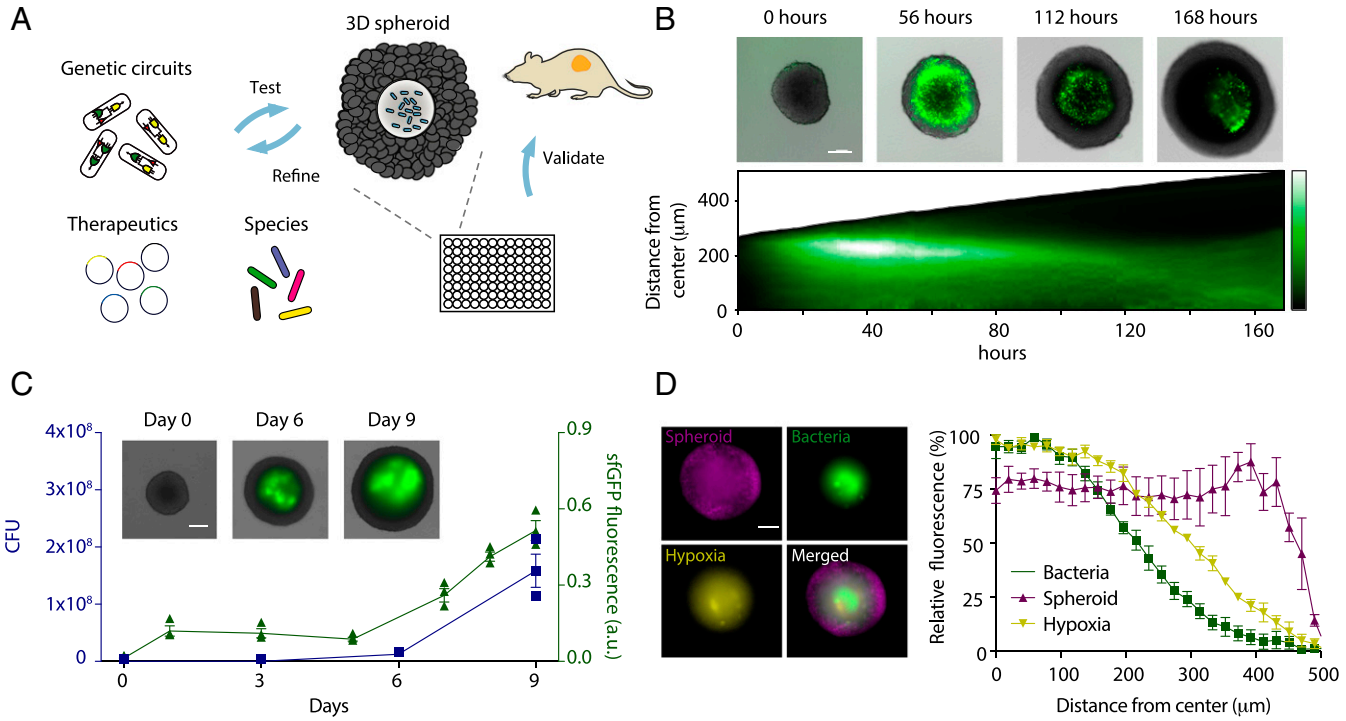

Fig. 1. Design and characterization of the BSCC platform. (*A*) Schematic of workflow for rapid testing of synthetic gene circuits, therapeutic payloads, and host species, using BSCC. Bacteria selectively colonize multicellular spheroids in vitro, where they are screened for growth, circuit dynamics, and therapeutic efficacy and then are validated in mouse tumor models. (*B*) *S. typhimurium* and tumor spheroid growth over time. (*Top*) Representative time series images of sfGFP expressing bacteria in CT26 tumor spheroids. (Scale bar, 200 μm.) (*Bottom*) The corresponding space-time diagram showing radially averaged fluorescence intensity of sfGFP-expressing bacteria. The gray boundary indicates the edge of the spheroid. (*C*) Total sfGFP of bacteria (green) and colony forming units (CFU, blue) over time. Day 0 values are after inoculation and washing of bacteria. Error bars indicate ± SE averaged over three measurements. a.u., arbitrary unit. (*Inset*) Representative images from this data. (Scale bar, 200 μm.) (*D*, *Left*) Spatial distribution of *S. typhimurium* in a spheroid 14 d post colonization. CT26 tumor spheroids (infrared fluorescent protein, magenta) develop hypoxic regions in the spheroid core shown by hypoxic probe dye (yellow). *S. typhimurium* (sfGFP, green) grow inside of the spheroid core. (Scale bar, 200 μm.) (*D*, *Right*) Distribution of fluorescence intensity of tumor cells, bacteria, and hypoxic regions from the center of spheroid. Error bars indicate ± SE averaged over three measurements.

Downloaded at Palestinian Territory, occupied on December 3, 2021
www.manaraa.com

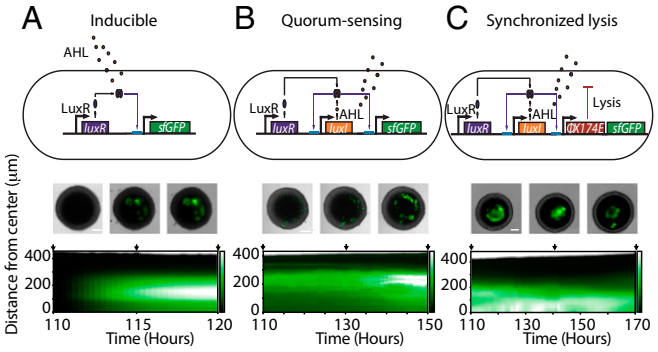

Fig. 2. Characterizing synthetic gene circuits using the BSCC platform. (*A*) Inducible circuit consisting of the *luxI* promoter driving sfGFP activated via externally supplied AHL. (*B*) Quorum-sensing (QS) circuit contains the *luxI* promoter regulated production of autoinducer AHL, leading to self-activation via positive feedback. (*C*) Synchronized lysis circuit (SLC) carries an additional lysis gene under the control of *luxI* promoter to achieve periodic lysis. (*Top*) Synthetic gene circuit diagrams. (*Middle*) Representative images of bacteria in tumor spheroids for each gene circuit. (Scale bar, 200 μm.) Regions outside of the field of view were filled with gray background color. (*Bottom*) Space-time diagram showing fluorescence intensity of sfGFP expressing bacteria radially averaged over time in spheroids. Black arrows correspond to images above. *LuxR* is constitutively expressed in all systems.

a critical density within the tumor core (26). After bacterial colonization of a spheroid, we observed a sharp increase in sfGFP production, demonstrating QS activation (Fig. 2*B*, *SI Appendix*, Fig. S3, and Movie S5). The maximum level of sfGFP reached was less than the inducible system (*SI Appendix*, Fig. S3), potentially because of lower levels of local AHL concentration. To enhance drug release from bacteria, we incorporated quorum-mediated bacterial lysis. We modified a recently created synchronized lysis circuit (SLC; Fig. 2*C*), which produces periodic cycles of self-lysis of host bacteria under QS control to efficiently release therapeutics into the surrounding environment (27). To minimize bacterial lysis before tumor colonization, we designed the circuit in a single operon on a low copy number plasmid. Following bacterial colonization of the spheroid, we observed fluctuations in fluorescence from SLC bacteria, indicating lysis (Fig. 2*C*, *SI Appendix*, Fig. S3, and Movie S6). In addition, spatiotemporal analysis indicated localization of bacteria closer to the center of the spheroid, whereas total sfGFP signal did not increase up to 170 h of bacterial colonization (Fig. 2*C* and *SI Appendix*, Fig. S4), suggesting a smaller and spatially restricted bacterial population resulting from a SLC. When gentamicin was removed from the media, we found that SLC was maintained inside spheroids twofold longer than a nonlysing inducible circuit (*SI Appendix*, Fig. S4), suggesting its use for biocontainment.

Screening Efficacy of Therapeutic Payloads in BSCC. Because the vast majority of bacterial therapy studies test a small number of therapeutic payloads that are rarely compared with one another (9), we sought to rapidly identify and compare bacterial therapeutics, using the BSCC platform. We created a library of therapeutics including previously uncharacterized bacterial toxins and anticancer peptides (*SI Appendix*, Table S2). Next, we tested bacterial therapies by selectively expressing therapeutics from bacteria within spheroids, using the inducible system. After adding AHL to spheroids that contain bacteria, we observed a varying degree of reduction in tumor spheroid size (Fig. 3*A*). The three candidates that exhibited the highest reduction in spheroid size were azurin (28), theta-toxin (29), and hemolysin E (30). The former is a proapoptotic protein, whereas the latter two are pore-forming toxins, of which theta-toxin has not yet been studied as an engineered bacterial therapeutic to our knowledge. Histopathological analysis of treated spheroids revealed higher levels of tumor cell death after treatment with bacteria expressing pore-forming toxins compared with treatment with control bacteria (*SI Appendix*, Fig. S5).

To compare the effects of genetic circuits on efficacy, we tested the effect of the therapeutic library across inducible, QS, and SLC systems in the BSCC platform. Incorporating the QS circuit into bacteria expressing the therapeutic library produced limited efficacy in tumor spheroids (Fig. 3*B*), corroborating our observation that quorum activation is limited and leads to reduced therapeutic production compared with the inducible circuit. In contrast, many therapeutics displayed significant efficacy when expressed from the SLC system on the same copy number plasmid as the QS circuit (Fig. 3*C*). Comparing across the therapeutic library, we identified theta-toxin as a potent therapy when combined with SLC, resulting in an ∼40% reduction in tumor spheroid size (Fig. 3*C*). Given the toxicity of theta-toxin to host bacteria (*SI Appendix*, Fig. S6), we varied AHL in the inducible circuit from 0 to 10 nM and found that decreasing inducer concentration did not increase efficacy (*SI Appendix*, Fig. S6). We reasoned that theta-toxin expression from SLC exhibited higher therapeutic efficacy compared with the inducible and QS circuit as a result of efficient release of therapeutics from the bacterial cytosol mediated by cell lysis.

Validating Efficacy of Bacterial Therapies in an Animal Model. To determine the predictive ability of the BSCC system, we assessed engineered bacteria in a syngeneic, hind-flank tumor mouse model harboring CT26 cells identical to those used to generate spheroids. We investigated inducible therapeutics with predicted high efficacy (azurin, theta-toxin, and hemolysin E), moderate efficacy (beta-hemolysin), and control (sfGFP). Approximately threefold reduced tumor growth was observed in vivo by bacterial therapeutics identified as highly effective from the in vitro screen compared with the control treatment (Fig. 3*D*). Tracking therapeutic responses over time revealed a high degree of similarity in trends of efficacy between BSCC and in vivo results (Fig. 3*E*). In contrast, results from bacteria cocultured with a monolayer of the same CT-26 cells failed to predict trends of efficacy in vivo (*SI Appendix*, Fig. S7). We performed histopathological analysis on treated tumors at trial termination. Consistent with the spheroid results, tumors treated with theta-toxin and hemolysin E showed increased cell death relative to tumors treated with control bacteria (*SI Appendix*, Fig. S8).

To improve efficacy, we next examined the QS and SLC circuits, as well as combination therapy in mouse tumor models. We found that efficacy of therapeutics expressed under SLC control in vivo corresponded to those from the spheroid screen (Fig. 3*F*). Comparing efficacy of SLC and QS circuits, theta-toxin from SLC exerted the strongest response, similar to the results from the BSCC platform (Fig. 3*G*). Furthermore, overall animal health, as measured by weight drop, improved with SLC compared with bacteria carrying inducible circuits, consistent with the observation of enhanced biocontainment by SLC in the BSCC platform (*SI Appendix*, Fig. S9). Leveraging the high-throughput capability of the BSCC, we also investigated combination therapy. Applying pairwise combinations of bacteria carrying inducible circuits at equal proportions in the BSCC, we found theta-toxin and azurin produced the most effective combination (Fig. 3*H*), exhibiting higher therapeutic efficacy than the additive effect of each individual therapy. This combination therapy in vivo exerted significantly stronger antitumor effects than either therapeutic alone, yielding a fourfold reduction in tumor size compared with control (Fig. 3*I*). These findings indicate the BSCC platform predictively identifies potent genetic circuits and therapeutic combinations in a highly parallel manner.

Expanding Applicability of BSCC to Diverse Bacterial Strains, Species, and Cell Types. Given that existing 3D coculture models for bacterial therapy are typically limited to particular types of bacteria

Downloaded at Palestinian Territory, occupied on December 3, 2021
www.manaraa.com

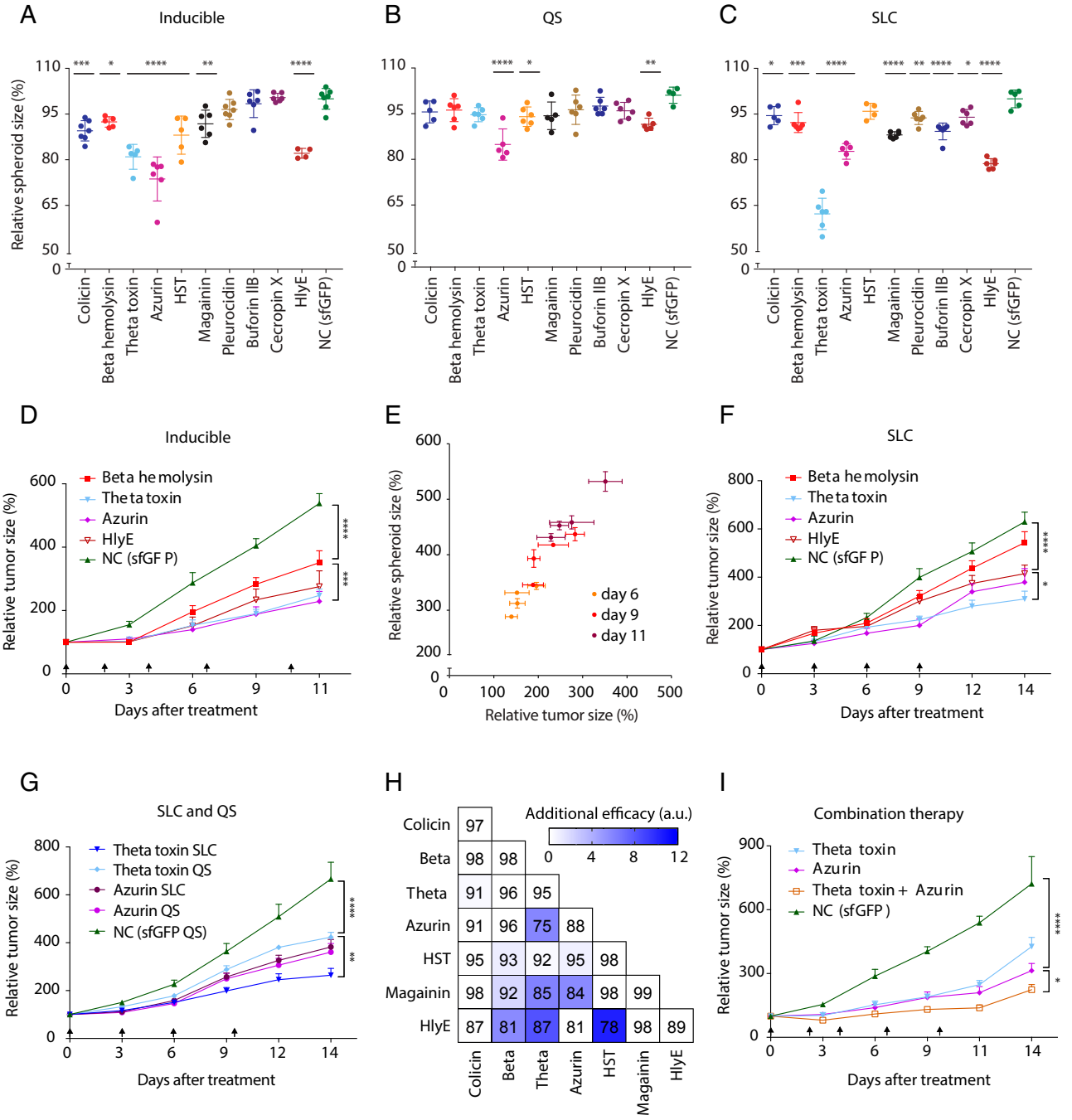

Fig. 3. Rapid screening of engineered bacterial therapeutics in the BSCC platform and assessment of efficacy in vivo. (*A–C*) Relative spheroid size 10 d post-administration of engineered *S. typhimurium* expressing various anticancer agents with an (*A*) inducible circuit after adding 10 nM AHL after bacteria colonization (****$P < 0.0001$, ***$P = 0.0002$, **$P = 0.0086$, *$P = 0.0301$ compared with control, one-way ANOVA with Bonferroni posttest), (*B*) quorum-sensing (QS) circuit (****$P < 0.0001$, **$P = 0.0022$; *$P = 0.0344$ compared with control, one-way ANOVA with Bonferroni posttest), and (*C*) SLC (****$P < 0.0001$, ***$P = 0.0005$, **$P = 0.0075$, *$P = 0.0394$ colicin, *$P = 0.0015$ cecropin X compared with control, one-way ANOVA with Bonferroni posttest). Values are normalized by control (bacteria expressing sfGFP). Error bars indicate ± SE averaged over four or more samples. HlyE, hemolysin E; HST, heat stable enterotoxin; NC, negative control. (*D*) Relative tumor size over time for s.c. CT26 tumor bearing mice injected with *S. typhimurium* carrying inducible gene circuit expressing beta hemolysin, theta-toxin, azurin, hemolysin E, and sfGFP (control) (****$P < 0.0001$, ***$P = 0.0003$, two-way ANOVA with Bonferroni posttest, $n = 8, 7, 10, 7, 5$ tumors, respectively, error bars show s.e.). (*E*) Analysis of correlation between relative tumor size over time in spheroid and in vivo model (linear regression, $R^2 = 0.92$). (*F*) Relative tumor size over time for s.c. CT26 tumor-bearing mice injected with bacteria carrying SLC-expressing beta hemolysin, theta-toxin, azurin, hemolysin E, and sfGFP (control) (****$P <$ 0.0001, *$P = 0.0363$, two-way ANOVA with Bonferroni posttest, $n = 8, 9, 6, 8, 8$ tumors, respectively; error bars show s.Ze.). (*G*) Relative tumor size over time for s.c. CT26 tumor bearing mice injected with *S. typhimurium* carrying SLC or QS circuit expressing theta-toxin, azurin, and sfGFP (control) (****$P < 0.0001$, **$P = 0.0018$, two-way ANOVA with Bonferroni posttest, $n = 8, 5, 10, 10, 9$ tumors, respectively; error bars show s.e.). Black arrows indicate bacteria injections in mice. (*H*) Efficacy of combinatorial therapy in the BSCC platform. The numbers in each box indicate average percentage spheroid size over two or more measurements 8 d post bacteria administration. Colors indicate additional efficacy of combinatorial therapy. Additional efficacy represents increased efficacy compared with additive effect alone (*Materials and Methods*). (*I*) Relative tumor size over time for s.c. CT26 tumor-bearing mice injected with *S. typhimurium* carrying inducible circuit expressing theta-toxin, azurin, combination (theta-toxin and azurin) and sfGFP (control) (****$P < 0.0001$; *$P = 0.0117$, two-way ANOVA with Bonferroni posttest, $n = 7, 9, 9, 5$ tumors respectively; error bars show s.e.).

MEDICAL SCIENCES
ENGINEERING
Downloaded at Palestinian Territory, occupied on December 3, 2021
www.manaraa.com

and cells (22, 31), we assessed the ability of the BSCC platform to coculture diverse bacterial strains, species, and host tissue types. First, we examined the colonization capacity and sfGFP expression level of clinically relevant strains of *S. typhimurium*: ELH430 (SL1344 *phoPQ*-), SL7207 (SL1344 *aroA*-), ELH1301 (SL1344 *phoPQ*-/*aroA*-) (32, 33), and VNP20009 (14028S *msbB*-/*purI*-), which has been used in clinical trials (23). All strains successfully colonized tumor spheroids, demonstrating stable coculture (*SI Appendix*, Fig. S10). ELH1301 exhibited the highest colonization and sfGFP expression levels within spheroids (*SI Appendix*, Fig. S10). Analysis of dynamics revealed increased initial invasion by ELH1301 compared with others (Fig. 4*A*), possibly contributing to its high colonization capacity at day 6. Next, we investigated colonization of *Listeria monocytogenes*, *Proteus mirabilis*, and *Escherichia coli*, bacterial species previously tested for cancer therapy (25, 34). Optimizing bacterial inoculation density, incubation time, and gentamicin concentrations (*SI Appendix*, Table S3), we established long-term growth of all bacterial species, indicated by an increase in sfGFP fluorescence and CFU from spheroids over multiple days (Fig. 4 *B*–*D*). Spatiotemporal analysis allowed for comparison of fluorescence distribution within spheroids and their respective dynamics. *L. monocytogenes* displayed a notably wide area of tumor colonization (Fig. 4*B*), possibly because of its cell-to-cell spreading ability within tumors (35). *P. mirabilis* reached the spheroid core at an earlier time compared with other bacteria (Fig. 4*C*), which might be attributable to its swarming ability. *E. coli* displayed a sharp increase in number at day 6 within the spheroid core (Fig. 4*D*), demonstrating similar dynamics to *S. typhimurium*. In addition to the ability to test host bacterial species, the BSCC platform can be used to study different tissue types. To do this, we generated spheroids derived from both human and mouse colorectal (HT29 and CT26/MC26) and breast (MCF7 and 4T1) cells. We observed increasing sfGFP fluorescence from *S. typhimurium* over time (*SI Appendix*, Fig. S11), demonstrating growth of bacteria in various cell lines. As efforts to integrate additional bacterial species for therapeutics continue to expand, we anticipate that the modularity of the BSCC system will allow a rapid evaluation of broad microbial therapies and diseases.

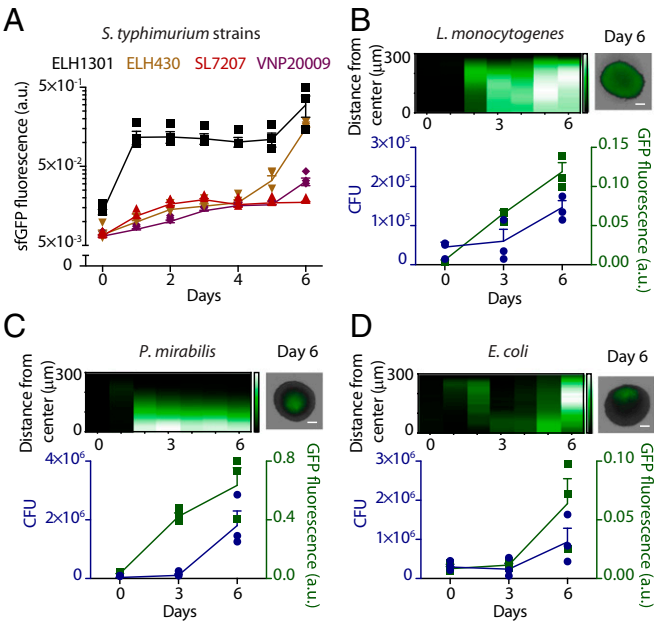

Fig. 4. Coculture of diverse bacterial strains and species in the BSCC platform. (*A*) sfGFP fluorescence of *S. typhimurium* strains within spheroids over time. (*B*–*D*) Colonization dynamics of (*B*) *L. monocytogenes*, (*C*) *P. mirabilis*, (*D*) *E. coli* within spheroids. (*Left*) Space-time diagram showing fluorescence intensity of sfGFP expressing bacteria radially averaged over time. (*Right*) Typical images of sfGFP expressing bacteria in spheroids 6 d after bacteria administration. (Scale bar, 100 μm.) (*Bottom*) Total sfGFP of bacteria (green) colony forming units (CFU, blue) over time. Day 0 values are after inoculation and washing of bacteria. (Scale bar, 100 μm.) a.u., arbitrary unit. Error bars indicate ± SE averaged over three measurements.

Discussion

We present an approach to simultaneously profile a vast number of engineered bacteria in a physiologically relevant, 3D multicellular system. By using a scalable methodology, the BSCC platform enables rapid build-test cycles of bacterial dynamics, therapeutics, and species for in vivo applications of synthetic biology. The key features of our system are quantification of bacterial population and circuit dynamics in a 3D disease model, accurate prediction of long-term disease progression in vivo from in vitro screening, and a simple and broadly applicable system for high-throughput development of novel bacteria therapies. The BSCC platform achieves these features through stable coculture with the use of gentamicin, a poorly diffusible antimicrobial agent that restricts growth of bacteria to within the spheroid core, analogous to in vivo bacterial containment in the tumor by the host immune system (36). The broad-spectrum activity of gentamicin (37) allows for investigation of diverse bacterial species.

One of the promising applications of the BSCC technology is the ability to rapidly screen large libraries of therapeutics expressed by bacteria circuit variants to narrow candidate selection for further development. Although previous studies have tested up to five bacteria-produced therapeutics in monolayers, using bacterial lysate and culture supernatants (38), the BSCC technology enabled screening of ∼40 bacterial therapy candidates for efficacy while simultaneously monitoring bacteria dynamics and disease progression over a timescale of weeks. This long-term monitoring aspect is critical to the success of bacterial therapies, as it is necessary to characterize the effects of dynamic therapeutic expression from genetic circuits on bacteria and cellular growth in physiological conditions.

In this study, we identified theta-toxin delivered by a lysis circuit, and combination therapy of theta-toxin and azurin, in *S. typhimurium* ELH1301 as efficacious bacterial therapies. By using the BSCC system, we found that although both SLC and QS circuits showed low therapeutic expression, the active cell lysis behavior in the SLC bacteria led to the therapeutic release from the bacterial cytosol, resulting in high efficacy compared with the QS circuit with no release mechanism. The reduction in tumor size observed was commensurate with standard-of-care chemotherapies in this rapidly growing colorectal cancer model (27, 39). In metastatic settings, the efficacy observed at this level could provide a clinically relevant benefit for patients, particularly in cases of chemoresistant or unresectable tumors (40). Because bacteria selectively colonize tumors, this targeted and controlled approach can deliver a broader range of therapeutics that can be toxic systemically and can improve efficacy and safety profiles.

In future studies, the platform can be used to screen even larger libraries and combinations of three to four agents, as often used in chemotherapy regimens to improve efficacy (41). Because multiple bacteria strains expressing different therapeutics will compete for resources within a tumor, reducing the effective dosage of each therapeutic, the BSCC system can assess how combination therapy will perform when increasing the number of bacterial therapies. In addition, the broad applicability of the spheroid model can be employed to assess combinations of bacterial therapy with chemotherapy (42) and radiotherapy (43) to improve on existing treatments. The BSCC system is precisely suited to quantitatively explore large libraries and combinatorial strategies in a high-throughput fashion.

Downloaded at Palestinian Territory, occupied on December 3, 2021
www.manaraa.com

Although we focused on cancer therapy in this study, the BSCC system may be expanded to characterize bacteria-based therapeutics for various diseases and to explore fundamental biological questions about bacteria in host tissue types. For example, the BSCC system may provide a platform to generally address safety concerns such as escape of bacteria from host tissue. Here BSCC may enable development and comparison of various biocontainment strategies such as antibiotic treatments (44) and genetic kill switch circuits (45). In addition, by incorporating immune cells into the coculture platform, the BSCC system may also be adapted to investigate bacteria-based immunotherapeutics that have been reported to augment immunotherapies (46, 47). Last, this multicellular spheroid model sets the stage for development of an organoid-based system that incorporates cells with different lineages and may enable further investigation of host–microbe interactions. As the field of engineered cell and microbial therapies evolves with the use of more complex synthetic gene circuits (48, 49) and incorporation of multicellular ecosystems (50), we envision the BSCC platform will accelerate therapeutic development for a wide range of diseases toward clinical translation.

Materials and Methods

All the materials and methods conducted in this study are detailed in *SI Appendix, Materials and Methods*: host strains and culturing, mammalian cells and spheroid generation, plasmids and therapeutic library constructions, bacteria coculture with tumor cell monolayer, bacteria coculture with tumor spheroids, bacterial colonization quantification via colony counts, microscopy, image alignment and localized fluorescence measurement for spheroids, sfGFP average fluorescence and radial histograms for spheroids, animal models, bacterial administration for in vivo experiments, tissue histological analysis, statistical analysis, and calculation of additional efficacy.

ACKNOWLEDGMENTS. We thank N. Arpaia, M. Omar Din, and J. Hasty for their helpful comments and suggestions. We thank the Herbert Irving Comprehensive Cancer Center Molecular Pathology Shared Resources Facility for help with histological sample processing. This work was supported in part by the Honjo International Foundation Scholarship (T.H.), NIH Ruth L. Kirschstein National Research Service Award (Z.S.S.), NIH Pathway to Independence Award (R00CA197649-02), Department of Defense (DoD) Idea Development Award LC160314, DoD Era of Hope Scholar Award BC160541, and NIH/National Cancer Institute Cancer Center Support Grant P30CA013696.

1. Riglar DT, et al. (2017) Engineered bacteria can function in the mammalian gut long-term as live diagnostics of inflammation. *Nat Biotechnol* 35:653–658.
2. Daeffler KN, et al. (2017) Engineering bacterial thiosulfate and tetrathionate sensors for detecting gut inflammation. *Mol Syst Biol* 13:923.
3. Hwang IY, et al. (2017) Engineered probiotic Escherichia coli can eliminate and prevent Pseudomonas aeruginosa gut infection in animal models. *Nat Commun* 8:15028.
4. Mao N, Cubillos-Ruiz A, Cameron DE, Collins JJ (2018) Probiotic strains detect and suppress cholera in mice. *Sci Transl Med* 10:eaao2586.
5. Liu Y, et al. (2018) Immunomimetic designer cells protect mice from MRSA infection. *Cell* 174:259–270 e11.
6. Teixeira AP, Fussenegger M (2017) Synthetic biology-inspired therapies for metabolic diseases. *Curr Opin Biotechnol* 47:59–66.
7. Isabella VM, et al. (2018) Development of a synthetic live bacterial therapeutic for the human metabolic disease phenylketonuria. *Nat Biotechnol* 36:857–864.
8. Anderson JC, Clarke EJ, Arkin AP, Voigt CA (2006) Environmentally controlled invasion of cancer cells by engineered bacteria. *J Mol Biol* 355:619–627.
9. Forbes NS (2010) Engineering the perfect (bacterial) cancer therapy. *Nat Rev Cancer* 10:785–794.
10. Danino T, et al. (2015) Programmable probiotics for detection of cancer in urine. *Sci Transl Med* 7:289ra84.
11. Riglar DT, Silver PA (2018) Engineering bacteria for diagnostic and therapeutic applications. *Nat Rev Microbiol* 16:214–225.
12. Bhatia SN, Ingber DE (2014) Microfluidic organs-on-chips. *Nat Biotechnol* 32:760–772.
13. Khademhosseini A, Langer R, Borenstein J, Vacanti JP (2006) Microscale technologies for tissue engineering and biology. *Proc Natl Acad Sci USA* 103:2480–2487.
14. Friedrich J, Seidel C, Ebner R, Kunz-Schughart LA (2009) Spheroid-based drug screen: Considerations and practical approach. *Nat Protoc* 4:309–324.
15. Clevers H (2016) Modeling development and disease with organoids. *Cell* 165: 1586–1597.
16. Breslin S, O'Driscoll L (2016) The relevance of using 3D cell cultures, in addition to 2D monolayer cultures, when evaluating breast cancer drug sensitivity and resistance. *Oncotarget* 7:45745–45756.
17. Fang Y, Eglen RM (2017) Three-Dimensional cell cultures in drug discovery and development. *SLAS Discov* 22:456–472.
18. Bhave MS, Hassanbhai AM, Anand P, Luo KQ, Teoh SH (2015) Effect of heat-inactivated Clostridium sporogenes and its conditioned media on 3-dimensional colorectal cancer cell models. *Sci Rep* 5:15681.
19. Goers L, Freemont P, Polizzi KM (2014) Co-culture systems and technologies: Taking synthetic biology to the next level. *J R Soc Interface* 11:20140065.
20. Kim HJ, Li H, Collins JJ, Ingber DE (2016) Contributions of microbiome and mechanical deformation to intestinal bacterial overgrowth and inflammation in a human gut-on-a-chip. *Proc Natl Acad Sci USA* 113:E7–E15.
21. Bartfeld S, et al. (2015) In vitro expansion of human gastric epithelial stem cells and their responses to bacterial infection. *Gastroenterology* 148:126–136 e6.
22. Osswald A, et al. (2015) Three-dimensional tumor spheroids for in vitro analysis of bacteria as gene delivery vectors in tumor therapy. *Microb Cell Fact* 14:199.
23. Toso JF, et al. (2002) Phase I study of the intravenous administration of attenuated Salmonella typhimurium to patients with metastatic melanoma. *J Clin Oncol* 20: 142–152.
24. Elsinghorst EA (1994) Measurement of invasion by gentamicin resistance. *Methods Enzymol* 236:405–420.
25. Chien T, Doshi A, Danino T (2017) Advances in bacterial cancer therapies using synthetic biology. *Curr Opin Syst Biol* 5:1–8.
26. Swofford CA, Van Dessel N, Forbes NS (2015) Quorum-sensing Salmonella selectively trigger protein expression within tumors. *Proc Natl Acad Sci USA* 112:3457–3462.
27. Din MO, et al. (2016) Synchronized cycles of bacterial lysis for in vivo delivery. *Nature* 536:81–85.
28. Yamada T, et al. (2002) Bacterial redox protein azurin, tumor suppressor protein p53, and regression of cancer. *Proc Natl Acad Sci USA* 99:14098–14103.
29. Verherstraeten S, et al. (2015) Perfringolysin O: The underrated Clostridium perfringens toxin? *Toxins (Basel)* 7:1702–1721.
30. Ryan RM, et al. (2009) Bacterial delivery of a novel cytolysin to hypoxic areas of solid tumors. *Gene Ther* 16:329–339.
31. Kasinskas RW, Forbes NS (2006) Salmonella typhimurium specifically chemotax and proliferate in heterogeneous tumor tissue in vitro. *Biotechnol Bioeng* 94:710–721.
32. Hoiseth SK, Stocker BA (1981) Aromatic-dependent Salmonella typhimurium are non-virulent and effective as live vaccines. *Nature* 291:238–239.
33. Hohmann EL, Oletta CA, Miller SI (1996) Evaluation of a phoP/phoQ-deleted, aroA-deleted live oral Salmonella typhi vaccine strain in human volunteers. *Vaccine* 14: 19–24.
34. Zhang H, et al. (2017) Proteus mirabilis inhibits cancer growth and pulmonary metastasis in a mouse breast cancer model. *PLoS One* 12:e0188960.
35. Tangney M, Gahan CG (2010) Listeria monocytogenes as a vector for anti-cancer therapies. *Curr Gene Ther* 10:46–55.
36. Westphal K, Leschner S, Jablonska J, Loessner H, Weiss S (2008) Containment of tumor-colonizing bacteria by host neutrophils. *Cancer Res* 68:2952–2960.
37. Edwards AM, Massey RC (2011) Invasion of human cells by a bacterial pathogen. *J Vis Exp* (49):2693.
38. Swofford CA, St Jean AT, Panteli JT, Brentzel ZJ, Forbes NS (2014) Identification of Staphylococcus aureus α-hemolysin as a protein drug that is secreted by anticancer bacteria and rapidly kills cancer cells. *Biotechnol Bioeng* 111:1233–1245.
39. Li W, Xu J, Zhao J, Zhang R (2017) Oxaliplatin and infliximab combination synergizes in inducing colon cancer regression. *Med Sci Monit* 23:780–789.
40. Shah SA, et al. (2007) Survival after liver resection for metastatic colorectal carcinoma in a large population. *J Am Coll Surg* 205:676–683.
41. Al-Lazikani B, Banerji U, Workman P (2012) Combinatorial drug therapy for cancer in the post-genomic era. *Nat Biotechnol* 30:679–692.
42. Dang LH, Bettegowda C, Huso DL, Kinzler KW, Vogelstein B (2001) Combination bacteriolytic therapy for the treatment of experimental tumors. *Proc Natl Acad Sci USA* 98:15155–15160.
43. Liu X, Jiang S, Piao L, Yuan F (2016) Radiotherapy combined with an engineered Salmonella typhimurium inhibits tumor growth in a mouse model of colon cancer. *Exp Anim* 65:413–418.
44. Zheng DW, et al. (2018) Optically-controlled bacterial metabolite for cancer therapy. *Nat Commun* 9:1680.
45. Lee JW, Chan CTY, Slomovic S, Collins JJ (2018) Next-generation biocontainment systems for engineered organisms. *Nat Chem Biol* 14:530–537.
46. Zheng JH, et al. (2017) Two-step enhanced cancer immunotherapy with engineered *Salmonella typhimurium* secreting heterologous flagellin. *Sci Transl Med* 9:eaak9537.
47. Gopalakrishnan V, et al. (2018) Gut microbiome modulates response to anti-PD-1 immunotherapy in melanoma patients. *Science* 359:97–103.
48. Weinberg BH, et al. (2017) Large-scale design of robust genetic circuits with multiple inputs and outputs for mammalian cells. *Nat Biotechnol* 35:453–462.
49. Nielsen AA, et al. (2016) Genetic circuit design automation. *Science* 352:aac7341.
50. Scott SR, et al. (2017) A stabilized microbial ecosystem of self-limiting bacteria using synthetic quorum-regulated lysis. *Nat Microbiol* 2:17083.

Downloaded at Palestinian Territory, occupied on December 3, 2021

www.manaraa.com